Center for Turbulence Research
Proceedings of the Summer Program 2012

Pressure-strain and near-wall modeling for two-dimensional separated flows

By C. L. Rumsey† AND E. Jeyapaul‡

Potential improvements are proposed to a two-equation explicit algebraic stress turbulence model applied to separated flows. These improvements include a specific dissipation rate equation found in the literature and a novel change to the pressure-strain modeling. For the two separated flows considered, the new pressure-strain model results in more negative Reynolds shear stress near the start of the separated shear layer, causing more energetic turbulence within the separation bubble and more accurate (earlier) reattachment. The new model yields significantly better agreement with large eddy simulation data and experiment.

1. Introduction

The Reynolds-averaged Navier-Stokes (RANS) equations have been used for many years to compute both attached and separated flows for aerodynamic applications. RANS methods have been very successful for attached flows in general, but their record for separated flows has been less consistent. In the early 1990s, two simple turbulence models were developed that improved the ability to predict separation location in many aerodynamic cases: the Spalart-Allmaras (SA) one-equation model (Spalart & Allmaras 1994) and the shear-stress transport (SST) two-equation model (Menter 1994). Today, these two models are available in most production CFD codes.

To date, more comprehensive RANS models, including full seven-equation second-moment Reynolds stress models (RSMs), have not gained widespread acceptance within the aerodynamics community. RSMs tend to be numerically stiff, and have not demonstrated superior capabilities compared to simpler one- or two-equation models for a wide enough range of cases. Explicit algebraic stress models (EASMs), which are derived from RSMs, have also been developed (e.g., Wallin & Johansson 2000; Gatski & Rumsey 2002). EASMs retain many of the advantages of their parent RSMs, require only two equations, and tend to be more robust than RSMs.

Among separated flows, there have been many documented cases for which RANS models like SA, SST, and EASM fail to adequately capture important flow physics. For example, for two-dimensional smooth-body separation over a hump (Greenblatt *et al.* 2006) or a hill (Frohlich *et al.* 2005), RANS models generally overpredict the extent of separation. As described in Wang *et al.* (2004) and Rumsey *et al.* (2006), this problem has been linked to underprediction of the turbulent shear stress in the separated shear layer, resulting in delayed reattachment/boundary-layer recovery. This deficiency is particular to RANS; eddy-resolving methods such as large eddy simulation (LES) can better predict the separated flow physics.

An ad hoc method for improving separated flow predictions in conjunction with k-ω models was explored in Rumsey (2009) with some success, but the method did not

† Senior Research Scientist, NASA Langley Research Center
‡ Postdoctoral fellow, NASA Langley Research Center

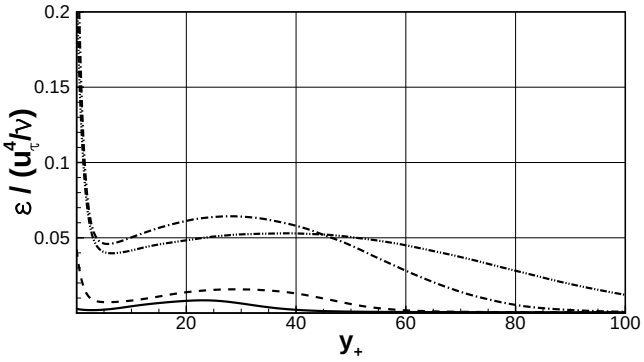

FIGURE 1. Dissipation magnitude at various locations relative to the start of the separation bubble from DNS of Marquillie *et al.* (2008); $(x - x_{sep})/(x_{reattach} - x_{sep}) = 8\%$ (solid), 46% (dash), 83% (dash-dot), 121% (dash-dot-dot). A rapid increase in near-wall dissipation is seen in the rear half and beyond the separation bubble.

demonstrate consistent improvement across a wide array of separated cases. The AJL-ω two-equation model of Abe *et al.* (2003) predicted the extent of the hill-flow separation well (see Wang *et al.* 2004), but as the AJL-ω model has not yet been widely implemented, it is not clear how well it works for other separated flows.

The current effort represents an examination of the "weak links" of RANS closure models to determine where future modeling efforts might most fruitfully be focused. Both near-wall effects as well as pressure-strain influence are examined. This work represents possible progress toward improved modeling, but it has not yet resulted in a final recommended form.

2. Near-wall modeling

Turbulent flow near walls is inhomogeneous and anisotropic, with Reynolds stresses approaching a two-component limit. RANS models require wall corrections to properly account for near-wall behavior. A review of the various single-point modeling approaches for near-wall corrections has been provided by Gerolymos *et al.* (2004) and Lai & So (1990). In the inner layer, the stresses are primarily influenced by the viscous diffusion, dissipation rate, and velocity-pressure gradient tensors. Specific to separated flows, there is a rapid increase in near-wall dissipation rate observed over the latter part of the separation bubble close to the reattachment location (see Figure 1). The importance of predicting this near-wall behavior on the ability to capture separation bubble size and recovery physics downstream is not yet clear.

To improve predictions of near-wall turbulence and document its influence on separated flow predictions, the homogeneous specific dissipation rate (ω_h) equation of Maduta & Jakirlic (2012)—designed to predict near-wall dissipation rate accurately—was investigated. The model was derived from the equation governing the homogeneous part of the total dissipation rate (ε_h), and is different from more standard ω-equation forms (e.g., Wilcox 2006), with

$$\frac{\mathcal{D}\omega_h}{\mathcal{D}t} = -(C_{\varepsilon 1}-1)\frac{\omega_h}{k}\overline{u_i u_j}\frac{\partial U_i}{\partial x_j} - (C_{\varepsilon 2}-1)\omega_h^2 + \frac{\partial}{\partial x_k}\left[\left(\frac{\nu}{2}+\frac{\nu_t}{\sigma_\omega}\right)\frac{\partial \omega_h}{\partial x_k}\right]$$
$$+ \underbrace{\frac{2}{k}\left(\frac{\nu}{2}+\frac{\nu_t}{\sigma_\omega}\right)\frac{\partial k}{\partial x_k}\frac{\partial \omega_h}{\partial x_k}}_{\text{Cross-diffusion}} - \frac{2}{k}\nu\left(\frac{\partial \overline{u_k u_i}}{\partial x_l}\frac{\partial^2 U_i}{\partial x_k \partial x_l} + C_{\varepsilon 3}\frac{1}{\omega_h}\frac{\partial \overline{u_k u_l}}{\partial x_j}\frac{\partial U_i}{\partial x_k}\frac{\partial^2 U_i}{\partial x_j \partial x_l}\right). \tag{2.1}$$

The coefficients in this equation are the same as those of the standard $k-\varepsilon$ turbulence model, with $\sigma_\omega = \sigma_\varepsilon = 1.1$, and $C_{\varepsilon 3}$=0.32. Maduta & Jakirlic (2012) used Eq. (2.1) in conjunction with a RSM. The objective here is to use it in combination with an EASM-based two-equation model with a standard k-equation. This proved to be problematic. The first issue was the stiffness near walls of the cross-diffusion term in Eq. (2.1). To circumvent this problem, the term was decomposed as

$$\frac{\partial k}{\partial x_k}\frac{\partial \omega_h}{\partial x_k} = \frac{\partial}{\partial x_k}\left(k\frac{\partial \omega_h}{\partial x_k}\right) - k\frac{\partial^2 \omega_h}{\partial x^2}.$$

Such treatment is not required for a similar term found in the SST and Wilcox (2006) models because the cross-diffusion term in those models is turned off near walls. In Eq. (2.1), it is active everywhere. This term switches sign very close to walls and hence becomes a sink; it is a source elsewhere. Although not shown, the DNS data of Marquillie *et al.* (2008) indicate the magnitude of the sink term grows rapidly in the reattachment region.

Even after alleviating the stiffness of the cross-diffusion term, the current approach was not successful in that it produced spuriously large eddy-viscosity levels that artificially suppressed separation. This non-physical result demonstrates the importance of treating any two-equation model as a system; one of the equations alone cannot be changed without consideration for the other. Future work will focus on possible remedies. The long-term goal is to combine near-wall model improvements with improvements to pressure-strain modeling, discussed in the next section.

3. Pressure-strain modeling

Starting from the SSG pressure-strain model of Speziale *et al.* (1991), the linearized form can be written (Gatski & Rumsey 2002):

$$\Pi_{ij} = -\left(C_1^0 + C_1^1\frac{\mathcal{P}}{\varepsilon}\right)\varepsilon b_{ij} + C_2 k S_{ij} + C_3 k\left(b_{ik}S_{kj} + S_{ik}b_{kj} - \frac{2}{3}b_{mn}S_{mn}\delta_{ij}\right)$$
$$- C_4 k\left(b_{ik}W_{kj} - W_{ik}b_{kj}\right), \tag{3.1}$$

where S_{ij} is the mean strain rate tensor, W_{ij} is the mean vorticity tensor, $\mathcal{P}/\varepsilon$ is the turbulent kinetic energy production over dissipation, and b_{ij} is the anisotropy tensor $b_{ij} \equiv \tau_{ij}/(2k) - \delta_{ij}/3$. The constants are $C_1^0 = 3.4$, $C_1^1 = 1.8$, $C_2 = 0.36$, $C_3 = 1.25$, and $C_4 = 0.4$. This is the model used to derive the EASM of Rumsey & Gatski (2003), which overpredicts separation bubble length, like other RANS models (Rumsey 2003). The EASM of Wallin & Johansson (2000) uses a modified form of the LRR pressure-strain model (Launder *et al.* 1975), and yields similar results. Below, we examine the influence of changes to the linearized SSG model on the ability to compute separated flows.

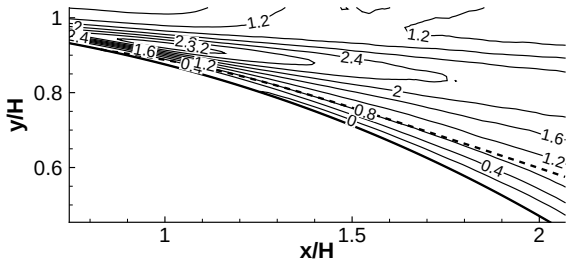

FIGURE 2. Contours of $\mathcal{P}/\varepsilon$ from Bentaleb *et al.* (2012) LES separated flow data on the back side of a rounded backstep. Zero-velocity streamline within separated zone is indicated by a dashed line.

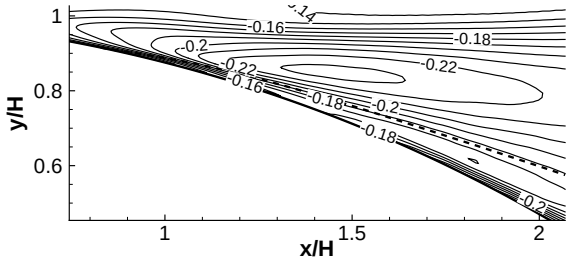

FIGURE 3. Contours of b_{12} from Bentaleb *et al.* (2012) LES separated flow data.

By examining LES and DNS data from hump-type flows, it is evident that the separated shear layer is far from equilibrium, in the sense that immediately following separation the $\mathcal{P}/\varepsilon$ is significantly higher than unity in the shear layer region. According to Bentaleb *et al.* (2012), this implies strong generation of streamwise fluctuations as a consequence of unsteady separation. It is an open question whether RANS can emulate this physical behavior in a Reynolds-averaged sense.

The constant coefficients in Eq. (3.1) were derived based on simple homogeneous flow considerations. The model is therefore unlikely to accurately predict non-equilibrium flows (Girimaji 2000). In order to determine a possible form that could yield improved predictions in the separated shear layer, we made use of LES data from Bentaleb *et al.* (2012), LES data from Frohlich *et al.* (2005), and DNS data from Marquillie *et al.* (2008). A plot of $\mathcal{P}/\varepsilon$ from the first reference is shown in Figure 2. Levels well above unity are present above the start of the separation bubble. As shown in Figure 3, this region is also associated with a local minimum in shear stress anisotropy b_{12}. The other LES and DNS cases with separation look similar.

As described in Wallin & Johansson (2000), EASMs differ substantially in their prediction of shear stress anisotropy b_{12} from linear eddy viscosity models, which assume constant values of C_μ such that $b_{12} = -C_\mu S_{12} k/\varepsilon$. Figure 4 shows b_{12} predictions as a function of Sk/ε, where $S \equiv \sqrt{S_{ij}S_{ij}/2}$. The EASM of Wallin & Johansson (2000) uses a modified form of the LRR pressure-strain model, whereas the EASM of Gatski & Rumsey (2002) uses linearized SSG. Both models are similar, achieving a near-constant level of b_{12} for $Sk/\varepsilon > 1.7$ (in the region where $\mathcal{P}/\varepsilon$ is greater than unity). Although not

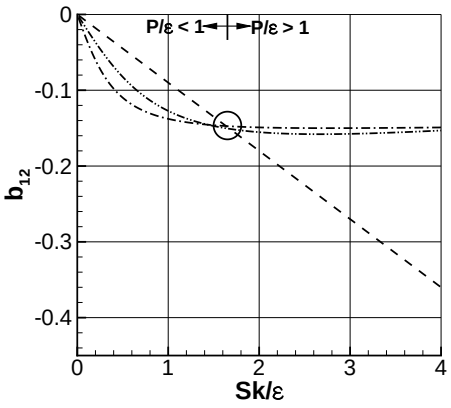

FIGURE 4. Anisotropy versus Sk/ε for parallel flow. Eddy viscosity model (dash), Wallin & Johansson (2000) (dash-dot), Gatski & Rumsey (2002) (dash-dot-dot). The circle represents the log-layer region.

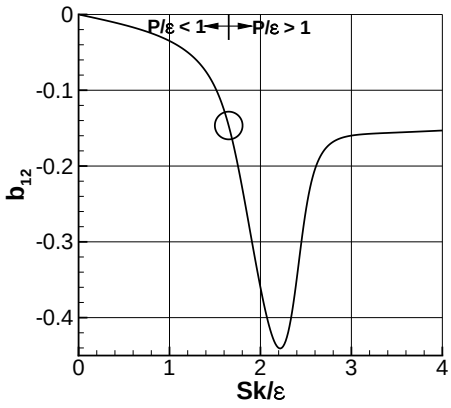

FIGURE 5. Anisotropy versus Sk/ε for parallel flow for the new model. The circle represents the log-layer region.

shown here, a similar effect is achieved by Menter's SST model through its use of the Bradshaw *et al.* (1967) assumption.

As shown earlier, the LES and DNS indicate that a region of local minimum b_{12} occurs near the start of the separation bubble, close to where $\mathcal{P}/\varepsilon$ exhibits a local maximum. In the current study, we modified the pressure-strain model in order to achieve this effect. This new model, described below, was designed to yield correct levels of b_{12} in the log layer as well as to revert to standard EASM behavior for high values of Sk/ε. However, for approximately $1.7 < Sk/\varepsilon < 3$, the new model yields more negative levels of b_{12} (even lower than linear eddy viscosity models), as shown in Figure 5. There is no particular significance to the minimum value of $b_{12} \approx -0.44$ attained by the model, other than the fact that values of this magnitude appear to be necessary to impact separated flow behavior. The current study's focus is primarily to document the influence of such a change, but the new model described does not represent a final recommended form.

The new EASM is achieved through a change in the pressure-strain model. The constant coefficient C_2 in Eq. (3.1) is replaced by C_2^*, which is a function of $\mathcal{P}/\varepsilon$:

$$C_2^* = C_2^R + (C_2 - C_2^R)f + C_S\frac{\mathcal{P}}{\varepsilon}(f-1), \tag{3.2}$$

where f is an ad hoc blending function that allows the model to revert to standard EASM for high values of Sk/ε,

$$f = \frac{1}{2}\left[1 + \tanh\left(C_a\frac{Sk}{\varepsilon} + C_b\right)\right]. \tag{3.3}$$

The resulting EASM used here is based on the k and ω equations, essentially the same as that described in Rumsey & Gatski (2003). The main exception is that the cubic equation solved for the variable coefficient $C_\mu^* \equiv \alpha_1/\tau$ is altered due to the above change in pressure-strain coefficient. The new cubic equation is

$$(\alpha_1/\tau)^3 + p(\alpha_1/\tau)^2 + q(\alpha_1/\tau) + r = 0, \tag{3.4}$$

where

$$p = -\frac{\gamma_1^*}{\eta^2\tau^2\gamma_0^*} + \frac{C_s(1-f)}{2\gamma_0^*}, \tag{3.5}$$

$$q = \frac{1}{(2\eta^2\tau^2\gamma_0^*)^2}\left(\gamma_1^{*2} - 2\eta^2\tau^2\gamma_0^* a_1^* - \gamma_1^*(1-f)C_S\eta^2\tau^2 - \frac{2}{3}\eta^2\tau^2 a_3^2 + 2\mathcal{R}\eta^2\tau^2 a_2^2\right), \tag{3.6}$$

$$r = \frac{\gamma_1^* a_1^*}{(2\eta^2\tau^2\gamma_0^*)^2}, \tag{3.7}$$

and $a_1^* = 2/3 - C_2^R/2 + (C_2^R - C_2)f/2$. All other variable definitions can be found in Rumsey & Gatski (2003). In the current model, $C_2^R = 1.2$, $C_S = 0.84$, $C_a = 4$, $C_b = -10$, and $\sigma_\omega = 1/0.65$. These constants were calibrated based on attached flow over a flat plate as well as several separated flows, including the two described in the next section.

This new model should be considered to be exploratory in nature, constructed to demonstrate the effect of making b_{12} more negative in separated shear layers through a modification to the pressure-strain model. More work is needed to insure that realizability and other important properties are satisfied (Girimaji 2000). If the effect is beneficial, this idea may lead to a more robust and systematic development of a useful pressure-strain model form.

4. Results

Two separated flow computations are shown here using CFL3D (Krist *et al.* 1998), a compressible upwind-biased finite-volume Navier-Stokes solver developed at NASA. The first is the flow over a rounded backstep, for which LES results of Bentaleb *et al.* (2012) were used for reference. The LES was computed with an incompressible solver, whereas the RANS used $M = 0.1$. Reynolds number based on step height (H) and upstream center-channel conditions was $Re_H = 13,700$. In the RANS, upstream conditions at the inflow boundary were set using LES data, and the top wall of the channel (at $y/H = 8.52$) used an inviscid wall boundary condition.

Figure 6 shows streamlines, indicating the separation bubble size and shape for standard EASM, the new EASM, and LES, respectively. Both RANS models separated at similar locations, in good agreement with LES, but standard EASM predicted a significantly delayed reattachment. Note that other RANS models (like SA and SST) have been tried for this case, and they yielded similar bubbles that were too long. In contrast, the EASM that used the modified pressure-strain model yielded a smaller bubble size, in better agreement with LES, although still somewhat too large. Skin friction, velocity profiles, and turbulent shear stress profiles are shown in Figures 7, 8, and 9, respectively. These indicate improved results compared to LES. In particular, the new model produced significantly higher magnitude peak turbulent shear stress within the bubble.

The second case is the flow over the baseline wall-mounted hump, with experimental data from Greenblatt *et al.* (2006). For this case, Mach number was $M = 0.1$ and Reynolds number based on hump chord (c) and upstream center-channel conditions was $Re_c = 936,000$. The upstream boundary was located so that a naturally developing

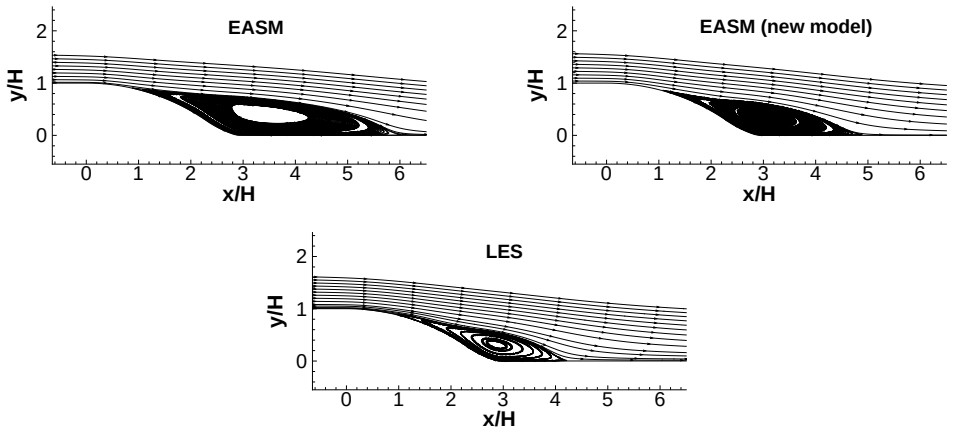

FIGURE 6. Streamlines for rounded backstep case of Bentaleb *et al.* (2012).

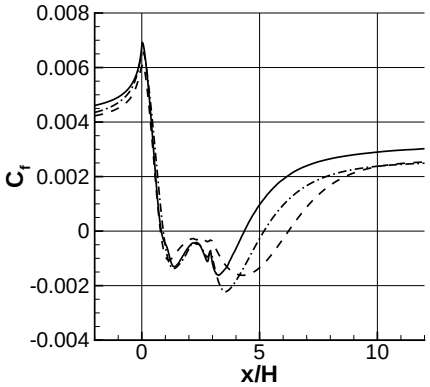

FIGURE 7. Wall skin friction coefficient for rounded backstep. LES (solid), standard EASM (dash), new EASM (dash-dot).

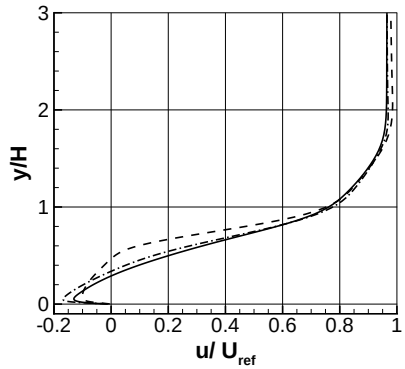

FIGURE 8. U-velocity for rounded backstep at $x/H = 3$. Line types same as previous figure.

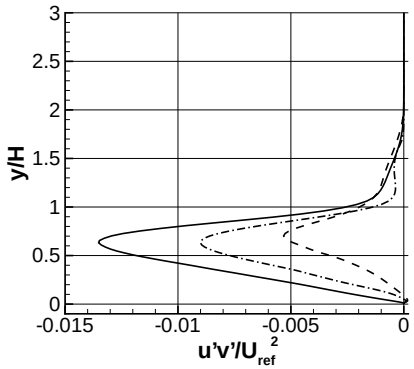

FIGURE 9. Turbulent shear stress for rounded backstep at $x/H = 3$. Line types same as previous figure.

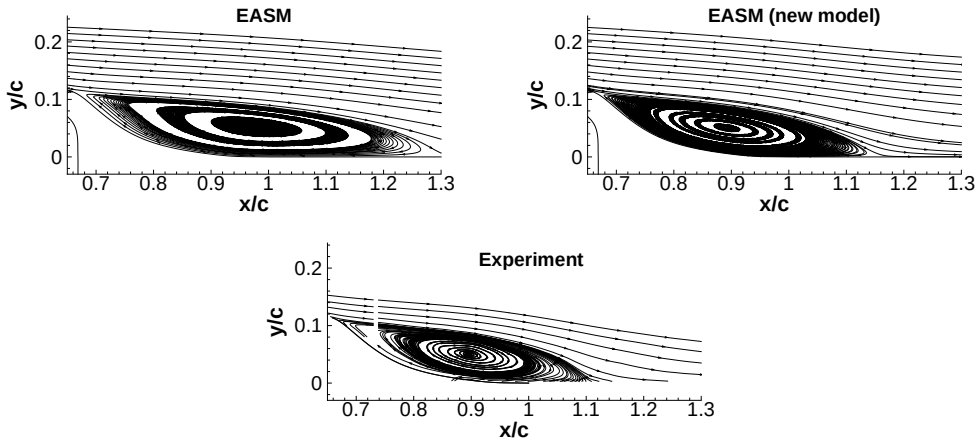

FIGURE 10. Streamlines for wall-mounted hump case of Greenblatt *et al.* (2006) (no flow–control case).

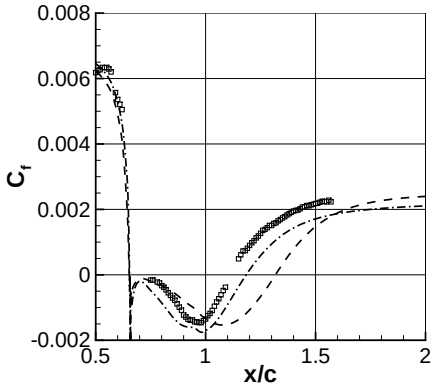

FIGURE 11. Wall skin friction coefficient for wall-mounted hump. Experiment (symbols), standard EASM (dash), new EASM (dash–dot).

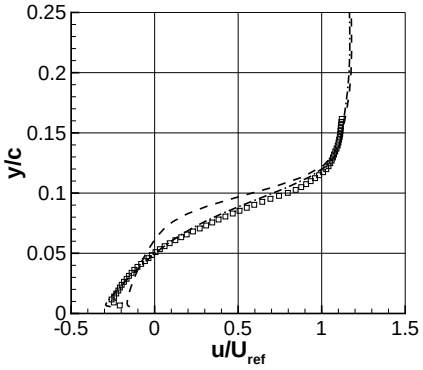

FIGURE 12. U-velocity for wall-mounted hump at $x/c = 0.9$. Line types same as previous figure.

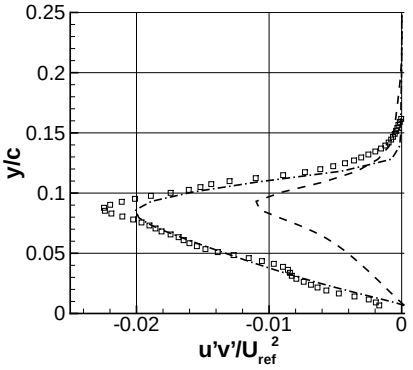

FIGURE 13. Turbulent shear stress for wall-mounted hump at $x/c = 0.9$. Line types same as previous figure.

boundary layer would approximately match experimental properties near $x/c = -2.14$. The top wall of the channel (near $y/c = 0.9$) used an inviscid wall boundary condition, and it was contoured to account for the influence of tunnel side-plate blockage in the experiment. This case has been widely computed; additional details can be found in Rumsey *et al.* (2006) or on the website http://cfdval2004.larc.nasa.gov.

Results are shown in Figures 10–13. Like the rounded backstep case, the standard EASM predicted too large a bubble. The new version with modified pressure-strain model significantly reduced the bubble size, in better agreement with experiment (although still somewhat too large). Most significantly, the new model produced turbulent shear stress levels in the bubble that agreed very well with experimental data.

5. Conclusions

Potential improvements to RANS models for computing separated flows were explored. A near-wall modeling idea from the literature has been identified as a possible source to improve the near-wall turbulence model behavior. It is anticipated that this (or similar) near-wall idea may eventually lead to improved two-equation EASMs.

Provisional changes to the pressure-strain model have significantly improved the ability of RANS models to compute 2-D separated flows. The altered pressure-strain model is currently implemented in an explicit algebraic stress model in k-ω form. The essence of the change is to make the Reynolds shear stress produced by the model more negative over a small range of production-over-dissipation levels exceeding unity. The increased turbulence production—also evident in LES and DNS data—is automatically activated near the start of separated shear layers. This exploratory work may suggest future systematic improvement of pressure-strain models applicable to separated flows.

Acknowledgments

The second author acknowledges the support of the NASA Postdoctoral Program, administered by Oak Ridge Associated Universities, during much of this work.

REFERENCES

Abe, K., Jang, Y.-J. & Leschziner, M. A. 2003 An investigation of wall-anisotropy expressions and length-scale equations for non-linear eddy-viscosity models. *Int. J. Heat and Fluid Flow* **24**, 181–198.

Bentaleb, Y., Lardeau, S. & Leschziner, M. A. 2012 Large-eddy simulation of turbulent boundary layer separation from a rounded step. *J. of Turbulence* **13** (4), 1–28.

Bradshaw, P., Ferriss, D. H. & Atwell, N. P. 1967 Calculation of boundary-layer development using the turbulent energy equation. *J. Fluid Mech.* **28** (3), 593–616.

Frohlich, J., Mellen, C. P., Rodi, W., Temmerman, L. & Leschziner, M. A. 2005 Highly resolved large-eddy simulation of separated flow in a channel with streamwise periodic constrictions. *J. Fluid Mech.* **526**, 19–66.

Gatski, T. B. & Rumsey, C. L. 2002 Linear and nonlinear eddy viscosity models. In *Closure Strategies for Turbulent and Transitional Flows* (ed. B. E. Launder & N. D. Sandham), pp. 9–46. Cambridge University Press.

Gerolymos, G., Sauret, E. & Vallet, I. 2004 Contribution to single-point closure

Reynolds-stress modelling of inhomogeneous flow. *Theoret. Comput. Fluid Dynamics* **17**, 407–431.

Girimaji, S. S. 2000 Pressure-strain correlation modelling of complex turbulent flows. *J. Fluid Mech.* **422**, 91–123.

Greenblatt, D., Paschal, K. B., Yao, C.-S., Harris, J., Schaeffler, N. W. & Washburn, A. E. 2006 Experimental investigation of separation control part 1: baseline and steady suction. *AIAA Journal* **44** (12), 2820–2830.

Krist, S. L., Biedron, R. T. & Rumsey, C. L. 1998 CFL3D user's manual (version 5.0). NASA/TM-1998-208444.

Lai, Y. G. & So, R. M. C. 1990 On near-wall turbulent flow modelling. *J. Fluid Mech.* **221** (1), 641–673.

Launder, B. E., Reece, G. J. & Rodi, W. 1975 Progress in the development of a Reynolds-stress turbulence closure. *J. Fluid Mech.* **41**, 537–566.

Maduta, R. & Jakirlic, S. 2012 An eddy-resolving Reynolds stress transport model for unsteady flow computations. In *Notes on Numerical Fluid Mechanics and Multidisciplinary Design, Vol. 117: Progress in Hybrid RANS-LES Modelling* (ed. F. Song, W. Haase, S.-H. Peng & D. Schwamborn), pp. 77–89. Springer-Verlag.

Marquillie, M., Laval, J.-P. & Dolganov, R. 2008 Direct numerical simulation of a separated channel flow with a smooth profile. *J. of Turbulence* **9** (1), 1–23.

Menter, F. R. 1994 Two-equation eddy-viscosity turbulence models for engineering applications. *AIAA Journal* **32** (8), 1598–1605.

Rumsey, C. L. 2003 Effect of turbulence models on two massively-separated benchmark flow cases. NASA/TM-2003-212412.

Rumsey, C. L. 2009 Exploring a method for improving turbulent separated-flow predictions with k-ω models. NASA/TM-2009-215952.

Rumsey, C. L. & Gatski, T. B. 2003 Summary of EASM turbulence models in CFL3D with validation test cases. NASA/TM-2003-212431.

Rumsey, C. L., Gatski, T. B., Sellers, W. L., Vatsa, V. N. & Viken, S. A. 2006 Summary of the 2004 computational fluid dynamics validation workshop on synthetic jets. *AIAA Journal* **44** (2), 194–207.

Spalart, P. R. & Allmaras, S. R. 1994 A one-equation turbulence model for aerodynamic flows. *Recherche Aerospatiale* **1**, 5–21.

Speziale, C. G., Sarkar, S. & Gatski, T. B. 1991 Modelling the pressure-strain correlation of turbulence: an invariant dynamical systems approach. *J. Fluid Mech.* **227**, 245–272.

Wallin, S. & Johansson, A. V. 2000 An explicit algebraic Reynolds stress model for incompressible and compressible turbulent flows. *J. Fluid Mech.* **403**, 89–132.

Wang, C., Jang, Y. J. & Leschziner, M. A. 2004 Modelling two- and three-dimensional separation from curved surfaces with anisotropy-resolving turbulence closures. *Int. J. Heat and Fluid Flow* **25**, 499–512.

Wilcox, D. C. 2006 *Turbulence Modeling for CFD, 3rd ed*. La Cañada, CA: DCW Industries, Inc.